coatings

MDPI

Article

Study of the Performance of Laser Melting Wear-Resistant Coatings on TC4 Titanium Alloy Surfaces

Gaosheng Wang [1,2,*], Jingang Liu [1,2,*], Jianhua Yang [1], Sisi Liu [1,2], Lei Bu [1] and Jianwen Chen [3]

[1] School of Mechanical Engineering and Mechanics, Xiangtan University, Xiangtan 411105, China
[2] Hunan Provincial Key Laboratory of Vehicle Power and Transmission System, Xiangtan 411104, China
[3] China North Industries Group Corporation, Jianglu Machinery Group Co. Ltd., Xiangtan 411100, China
* Correspondence: wgs@hnie.edu.cn (G.W.); liujingang@xtu.edu.cn (J.L.)

Abstract: To improve the wear resistance of TC4 titanium alloy, two types of wear-resistant coatings were applied to the surface using laser melting: Ni60 + 50% WC and d22 powder priming. The phase composition and microstructure of the coatings were characterized by X-ray diffractometry (XRD), scanning electron microscopy (SEM), and energy spectroscopy (EDS). The mechanical properties of the coating were tested using an HV-1000 micro-Vickers hardness tester, an HRS-2M high-speed reciprocating friction and wear tester, and a WDW-100D electronic universal testing machine. The results show that Ni60 + 50% WC composite coating and d22 priming + (Ni60 + 50% WC) composite coating mainly consist of W_2C, TiC, $Ni_{17}W_3$, Ni_3Ti, and Ti_xW_{1-x} phases. Compared to the TC4 substrate, the microhardness of both coatings is significantly higher, approximately 2.8 times the microhardness of the substrate. In frictional wear experiments, the average friction factors of the two coatings and the TC4 substrate are 0.476, 0.55, and 0.865, respectively, and the wear of the two coatings is only 0.0559–0.0769 that of the TC4 substrate, with a significant increase in wear resistance, nearly 17 times higher than that of the substrate. The coating shows flaking, shallow abrasion marks, and granular debris, dominated by adhesive wear and fatigue wear, while the TC4 substrate shows more furrows on the surface, dominated by abrasive wear. The shear bond strengths of the Ni60 + 50% WC composite coating and the d22 powder primed + (Ni60 + 50% WC) composite coating were 188.19 MPa and 49.11 MPa, respectively. Conclusion: both coatings significantly improve the hardness and wear resistance of the TC4 titanium alloy substrate surface, with the Ni60 + 50% WC composite coating performing better in hardness, wear resistance, and bond strength.

Keywords: laser cladding; titanium alloy; microstructure; microhardness; wear amount; abrasion resistance

Citation: Wang, G.; Liu, J.; Yang, J.; Liu, S.; Bu, L.; Chen, J. Study of the Performance of Laser Melting Wear-Resistant Coatings on TC4 Titanium Alloy Surfaces. *Coatings* **2024**, *14*, 730. https://doi.org/10.3390/coatings14060730

Academic Editor: Angela De Bonis

Received: 30 April 2024
Revised: 25 May 2024
Accepted: 29 May 2024
Published: 7 June 2024

1. Introduction

Titanium alloys are widely used in the aerospace, petrochemical, automotive, and biomedical industries for their low density, high specific strength, high-temperature resistance, and corrosion resistance [1,2]. However, the disadvantages of titanium alloys, such as low hardness and poor wear resistance, limit their further application [3,4]. To solve this problem, the surface properties of titanium alloys are improved with ceramic–metal composite coatings that have a combination of high hardness and high wear resistance [5,6]. Laser cladding is widely used to enhance titanium's tribological properties and expand titanium's industrial applications due to its high energy density, low dilution, and good metallurgical bonding of the coating to the substrate [7].

Laser cladding materials are often selected from hard particle-reinforced Ni-, Co-, or Fe-based self-fusing alloy powders such as TiC, SiC, and WC to form ceramic–metal composite coatings [8,9]. Ni-based alloy powders are the most widely studied and used as laser cladding materials due to their excellent wear resistance and moderate price [10]. Compared to other ceramic powders such as TiC and SiC, WC not only has a coefficient

of thermal expansion similar to that of titanium alloys, but also has excellent properties such as high hardness and good wettability with Ni-based alloys, and is considered to be a useful reinforcing material for wear-resistant coatings on titanium alloys [11,12]. Currently, scholars at home and abroad have conducted relevant research on the wear resistance of laser cladding WC reinforced Ni-based alloy powder composite coatings. Chen et al. [13] studied the use of nickel-based alloy Deloro-22 for powder-blown laser cladding, and modified the surface of Ti-6Al-4V bars to TiNi/Ti2Ni-based intermetallic composites to improve the surface properties of Ti-6Al-4V. The results indicated that Deloro-22 nickel alloy powder can modify the Ti-6Al-4V surface by synthesizing various types of Ti_xNi_y through laser processing. Chen Yonggang [14] studied the wear resistance of WC particle-reinforced Ni-based alloy coatings and showed that the composite layer with a volume fraction of 50% WC + Ni60 has the best wear resistance, with seven times the wear resistance of a 45-steel matrix. The coating interface is well bonded and the metallography is uniform and dense, despite some microscopic defects such as holes in the coating. Guo et al. [15] studied the effect of WC content on the structure and wear resistance of laser-melting clad Ni-based alloy coatings. The results showed that the average hardness and wear resistance of the clad layer increased as the WC content increased. When the WC mass fraction is increased to 50%, the average hardness of the clad layer can reach 1200 HV. This is approximately five times the hardness of the stainless-steel matrix, with the lowest wear rate. However, the composite coating at 50% WC has some defects such as holes and cracks. Fernández et al. [16] investigated the tribological properties of Ni-based coatings reinforced with different levels of WC (0%–50%) and found that wear decreased exponentially with increasing WC content, with the main wear mechanisms being adhesive wear, oxidation, and abrasive wear. However, defects such as holes and cracks were still observed in the 50% WC composite coating.

A comprehensive study of the above can reveal that Ni-based + 50% WC composite coatings are used for surface treatment of metallic materials such as carbon steel, 45 steel, and stainless steel due to their high hardness and excellent wear resistance. Still, defects such as porosity and cracks inevitably exist. At present, there are relatively few systematic studies on the structure and wear resistance of Ni-based + 50% WC composite coatings. Research on TC4 titanium alloys has not yet been fully developed. Therefore, this paper proposes two composite layers, Ni60 + 50% WC and d22 powder priming + (Ni60 + 50% WC), to improve the wear resistance of TC4 titanium alloy and to compare the microstructure and mechanical properties of the two coatings.

2. Experimental Procedure

2.1. Experimental Materials

The tests were carried out using 100 mm × 50 mm × 10 mm TC4 titanium alloy base material, and three powders—Ni60, WC, and deloro22—were selected as the cladding materials. Table 1 shows the chemical composition of the TC4 titanium alloy matrix and the three cladding materials. Mix the powder in a 50% ratio using a 500 mL stainless steel grinding tank, with stainless steel balls of different diameters as the grinding medium. Dry grinding is carried out in a planetary ball mill (QM-3SP2 type), with a ball-to-material ratio of 20:1. After loading, the filling rate of the grinding tank is about 20%, with a speed of 500 rpm. After 30 min of grinding, stop for 6 min to avoid overheating of the grinding tank, and mix for 10 h to ensure uniform mixing of the powder. After mixing, the powder is put into a vacuum dryer at 100 °C for 1.5 h to dry before use.

Chemical composition of TC4 titanium alloy is shown in Table 1.

Table 1. Chemical composition of base material and cladding material (Wt.%).

TC4 titanium alloy	Element	Al	V	Si	Fe	C	N	H	O	Ti
	TC4	6.5	4.3	0.03	0.096	0.01	0.013	0.0048	0.05	Bal
WC alloy powder	Element	WC	Fe	Co	Cu	Si	Al	C	O	
	WC	Bal	0.1	0.05	0.001	0.001	0.015	0.05	0.3	
Ni60 alloy powder	Element	C	Cr	Si	W	Fe	Ni	B		
	Ni60	0.8	15.5	4	3	15	Bal	3.5		
deloro22 alloy powder	Element	C	Cr	Si	Mn	Fe	Ni	B		
	Ni60	0.2	0.1	2.85	0.5	0.5	Bal	1.45		

2.2. Laser Cladding Experiment

Before the test, the spare titanium alloy specimens were coarsely ground with 400- and 600-grit sandpaper and cleaned with alcohol to remove surface oils, then cleaned with acetone in an ultrasonic cleaner and dried with a hair dryer. The laser cladding equipment uses GS TFL-H1000CO2 laser equipment GSTFL-H10000CO2 laser provided by Wuhan Dazu Jinshikai Laser System Co., Ltd. in Wuhan, China, the powder feeding method is synchronous powder feeding, and the protective gas is argon; the schematic diagram is shown in Figure 1. The laser coating process parameters are as follows: laser power of 2200 W, spot diameter of 5 mm, scanning speed of 6 mm/s, and powder feed of 20 mg/s, resulting in a specimen with a coating thickness of around 1.2–1.5 mm, and the thickness of the d22 base layer is about 0.6 mm. When the WC concentration rises above 30%, cracking of the deposited layer occurs [17]. To avoid this, the TC4 titanium alloy substrate is preheated to 500 °C before laser cladding.

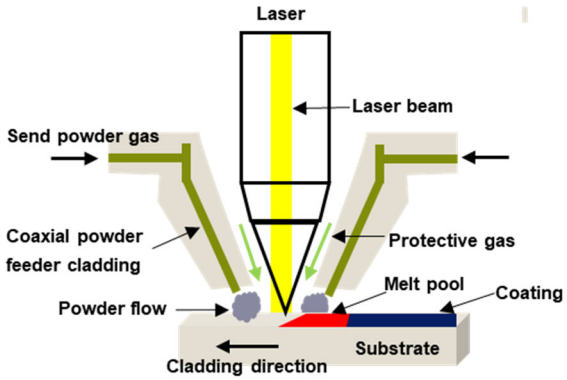

Figure 1. Principle diagram of laser cladding.

2.3. Microstructural Characterization

After laser cladding, specimens of size 10 mm × 10 mm × 10 mm were cut by an EDM wire cutter and sequentially ground using 400, 600, 800, 1000, 1500, and 2000 grit SiC sandpaper, followed by polishing using a diamond suspension with a grain size of 1 μm. The samples were polished and subjected to 1HF:3HNO_3:20H_2O corrosive solution for 20 s. The phase composition of the coating was examined using X-ray diffraction (XRD) over a range of 5–90° at a scanning speed of 10°/min. Scanning electron microscopy (SEM) and energy dispersive spectroscopy (EDS) were used to characterize the microstructure of the coating.

2.4. Performance Tests

The microhardness of the coating cross-section was tested using an HV-1000 micro-Vickers HV-1000 Vickers microhardness tester produced by Shanghai Yizong Precision Instrument Co., Ltd., Shanghai, China, hardness tester with a load of 1.96 N and a holding time of 10 s. The HRS-2M high-speed reciprocating friction and wear tester was used

to conduct dry sliding friction-wear test on TC4 titanium alloy substrate and coating at room temperature. The experimental object is a 6 mm diameter carbide YG6 tungsten carbide steel ball, the applied load is 90 N, the running length is 5 mm, the rotation radius is 5 mm, the speed is 600 r/min, and the test time is 30 min. The principle diagram of the friction-wear test is shown in Figure 2.

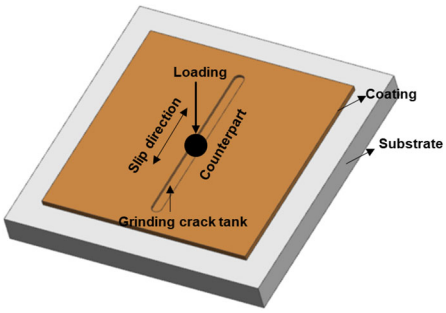

Figure 2. Principle diagram of the frictional wear test.

2.5. Bond Strength Test

As the thickness of the coating is substantial at 1.2–5 mm, which is a thick coating, the shear method is selected to measure the bonding strength of the coating. When the shear force at the interface between the coating and the substrate causes the coating to peel off from the substrate, the magnitude of the shear force per unit area is used to characterize the bonding strength of the coating. The test is conducted using an electronic universal testing machine. The fixture holding the sample is placed on a designated workbench. With the aid of a computer, the load applied to the fixture is controlled and the relationship between load and displacement is observed. The test equipment is shown in Figure 3.

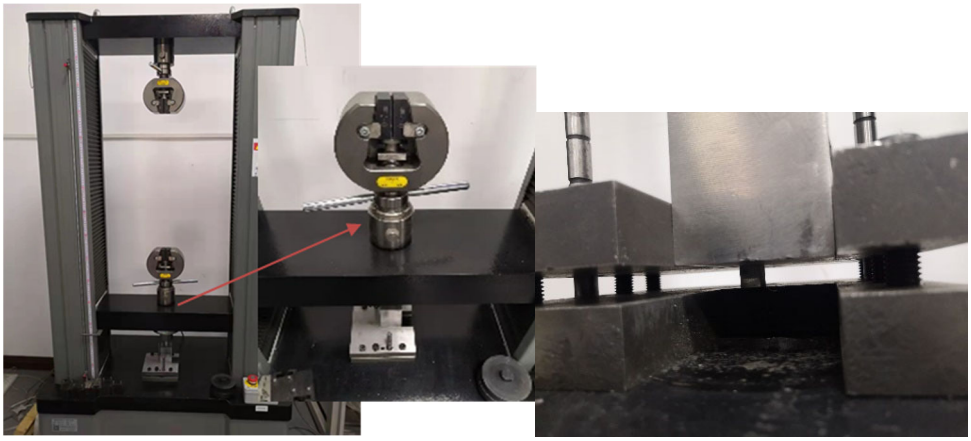

Figure 3. Shear test process diagram.

3. Results and Discussion

3.1. X-ray Diffraction Analysis

The X-ray diffraction patterns of the coatings are shown in Figure 4. The Ni60 + 50% WC coating and the d22 primed + (Ni60 + 50% WC) coating consist mainly of W_2C, TiC, $Ni_{17}W_3$, Ni_3Ti, and Ti_xW_{1-x} phases. The differences in the intensities of TiC and $Ni_{17}W_3$ in the Ni60 + 50% WC coating and the d22 substrate + (Ni60 + 50% WC) coating are mainly due to the presence of the substrate layer, which affects the cooling rate of the coating, element diffusion, interfacial bonding, residual stress, heat treatment and cooling rate, and their interactions. Due to the relatively high laser power of 2200 w, a large part of the WC powder was melted and decomposed into W and C elements in the melt pool, which formed an in situ enhanced phase in the coating during the rapid solidification process.

Because Ti and W have a strong "affinity" for C, they react easily to form the in situ carbides TiC and W_2C. In addition, the TC4 titanium alloy matrix and cladding material are melted, and a large number of elements diffuse into the molten pool. During the rapid solidification process, various elements interact to form phases such as Ni_3Ti and $Ni_{17}W_3$. Both of the two composite coatings have a solid solution phase and carbide phase, which can make the coatings have high hardness and wear resistance.

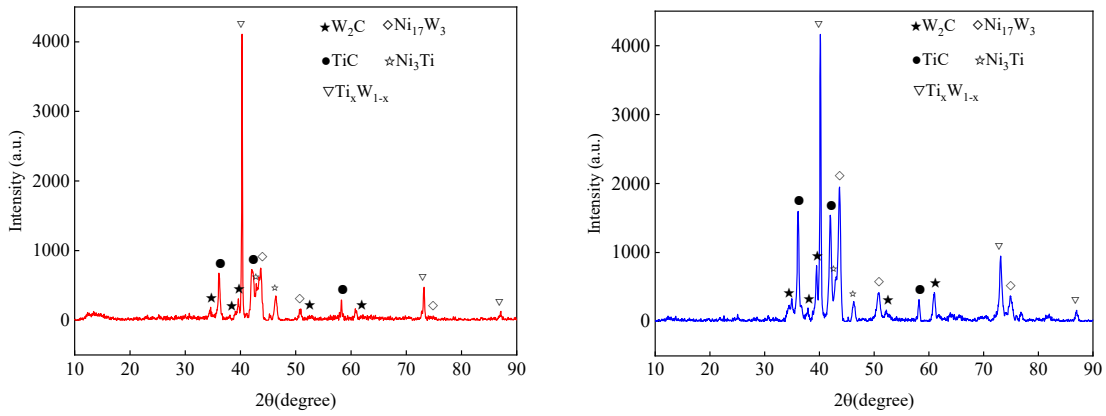

Figure 4. X-ray diffractogram of the coating. (**a**) Ni60 + 50% WC. (**b**) d22 priming + (Ni60 + 50% WC).

3.2. Microstructure Analysis

Figure 5 shows the macroscopic morphology of the Ni60 + 50% WC and d22 primer + (Ni60 + 50% WC) composite coatings. From the figure, it can be observed that the microstructure of the two coatings is uniform and dense. The Ni60 + 50% WC composite coating does not have obvious cracks and pore defects, while the d22 primer + (Ni60 + 50% WC) composite coating does not have crack defects but has obvious pores. The formation of pores in the d22 substrate + (Ni60 + 50% WC) composite coating is mainly due to the presence of the substrate affecting the deposition and cooling process of the overall coating, interface reactions, differences in thermal expansion coefficients, surface roughness, and wettability. These factors work together to form pores in the overlying layer.

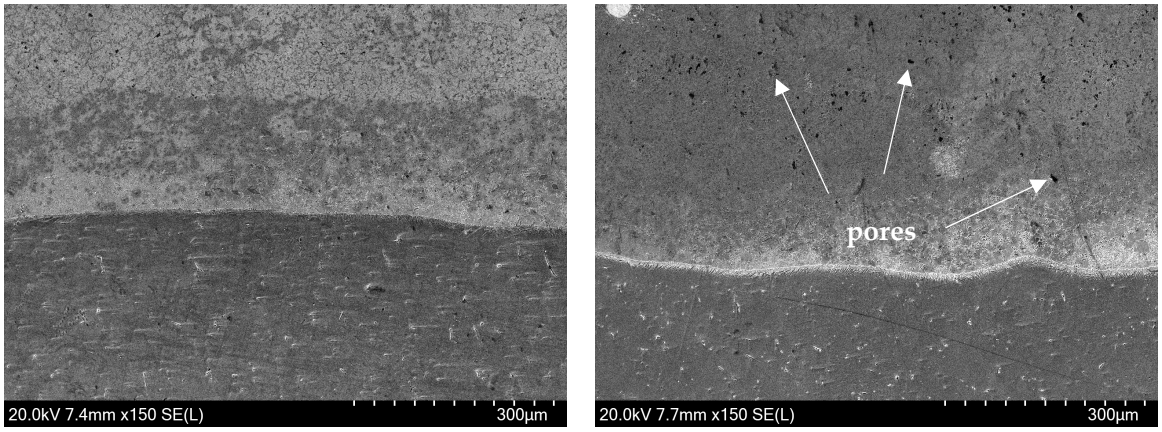

Figure 5. Macro morphology of coatings. (**a**) Ni60 + 50% WC. (**b**) D22 primer + (Ni60 + 50% WC).

The SEM morphology of the transverse section of the clad coating is shown in Figure 6. From Figure 6a,c, the coating is homogeneous and dense, with no obvious microscopic defects such as cracks and holes. A distinctive bright white band was observed on the underside of each coating, indicating a good metallurgical bond between the coating

and the substrate. At a crystalline level, the "bright white band" at the bottom of the coating can be explained as an interfacial region where the crystals of the coating material and the substrate material intersect. During the coating preparation process, diffusion of elements and chemical reactions between the coating and substrate materials at elevated temperatures leads to a mixing and rearrangement of crystal boundaries. This interfacial region of crystal boundary mixing appears as a bright white band in SEM images, indicating a well-established crystal boundary bonding between the coating and substrate. This crystal boundary bonding not only increases the contact area between the coating and substrate, but also enhances the bonding strength and wear resistance. Thus, from a crystalline perspective, the "bright white band" at the bottom of the coating reflects the interfacial region of crystal boundary mixing formed between the coating and substrate, which is crucial for improving the bonding quality and performance of the coating. In addition, it can be observed that there is a staggered pattern between the coating and the substrate, and some structures in the coating insert into the substrate-like wedges, indicating that both coatings can produce excellent metallurgical bonding with the substrate and this structure can provide sufficient strength at the bonding interface. Due to the high instantaneous energy of the laser beam, the pre-set powder melts rapidly, and metallurgical bonding between the powder and the substrate occurs and then solidifies. In contrast, the fusion line in the d22 primed + D22 primed + (Ni60 + 50% WC) composite coating is clearer (Figure 6c), and the microstructure is more uniform and dense. In addition, the matrix in the vicinity of the fusion line for all coatings is characterized by acicular martensite due to a higher cooling rate than the critical cooling rate in the heat-affected zone (HAZ) [18].

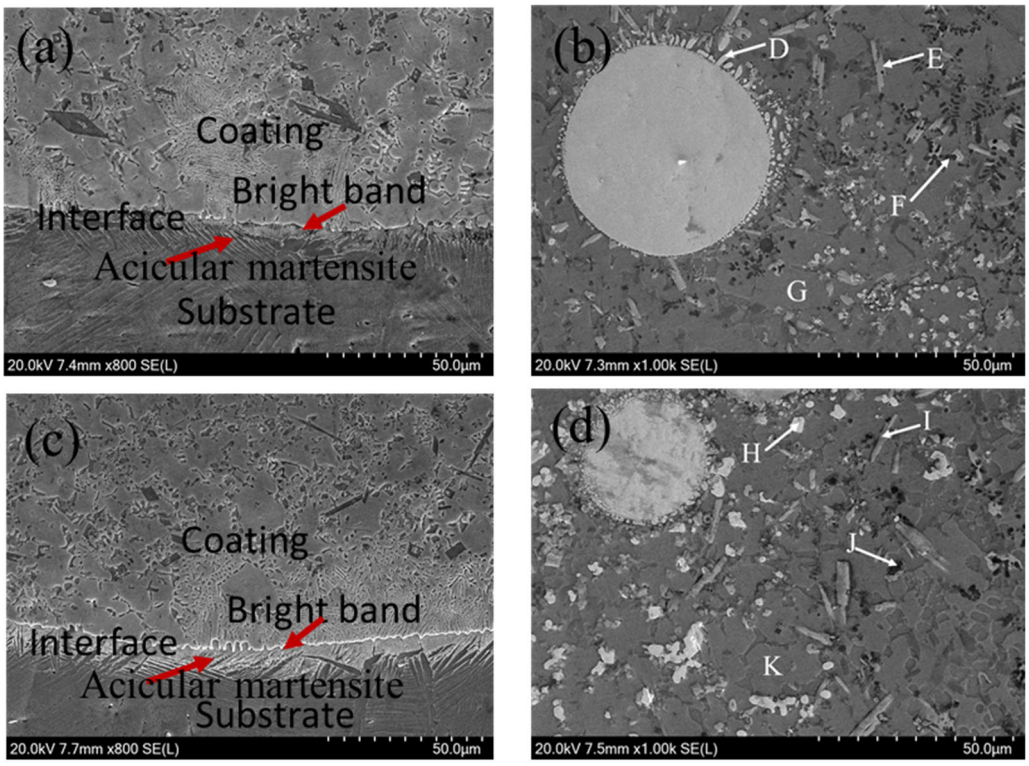

Figure 6. (**a**,**c**) Microstructures near the bottom area of the coating and (**b**,**d**) EDS point analyses near the enlarged area in the middle of the coating, where (**a**,**b**) are Ni60 + 50% WC composite coatings and (**c**,**d**) are d22 primed + (Ni60 + 50% WC) composite coatings.

To determine its phase composition in the coating, the structure of the middle region of the layer was spot-swept using an energy spectrometer, as shown in Figure 6b,d, and combined with XRD (Figure 4) and EDS results (Table 2) to analyze the tissue composition. The microstructure of both coatings can be observed in the diagram as irregular white

tissue (D, H) consisting mainly of elements W and C, which is presumed to be W2C; there is also light gray rod-like tissue (E, I), black spherical tissue (F, J) and dark gray tissue (G, K). E and I, characterized by a light gray rod-like structure, are mainly composed of W, C, and Ti elements, with the elemental ratio of C to Ti close to 1:1. Presumably, this structure is TiC; F, J is mainly composed of Ti, Ni, with an elemental ratio of approximately 1:3, which can be inferred to be Ni_3Ti; G, K is mainly composed of W, Ti, Ni, and a few other elements in which Ni is present at a high content, and other elements such as C, Cr, and Si are also detected; presumably, this tissue mainly contains Ti_xW_{1-x} and $Ni_{17}W_3$.

Table 2. EDS analysis of the central area of the coating.

Point	Composition (wt.%)									
	W	**C**	**Ti**	**Ni**	**V**	**O**	**Cr**	**Si**	**B**	**N**
D	80.18	11.57	1.58	4.98	—	—	—	1.69	—	—
E	51.74	10.18	11.56	6.18	4.75	1.78	1.03	1.61	11.17	—
F	0.84	6.03	18.35	48.94	—	19.19	—	—	—	6.65
G	6.83	7.60	15.85	66.93	1.44	—	1.35	—	—	—
H	80.01	12.57	1.11	4.36	—	—	—	1.95	—	—
I	50.96	11.73	13.08	6.94	3.94	1.63	1.19	1.49	9.04	—
J	3.84	13.53	16.83	54.85	—	9.65	—	1.30	—	—
K	6.93	5.16	21.46	53.01	2.20		1.91	5.86	—	3.47

In order to verify the bonding of the substrate and the coating, and to qualitatively analyze the diffusion of the elements in the substrate and the layer, a line scan of the Ti and Ni elemental content of the layer was performed on both coating cross-sections with the substrate as the starting point perpendicular to the interface direction, as shown in Figure 7.

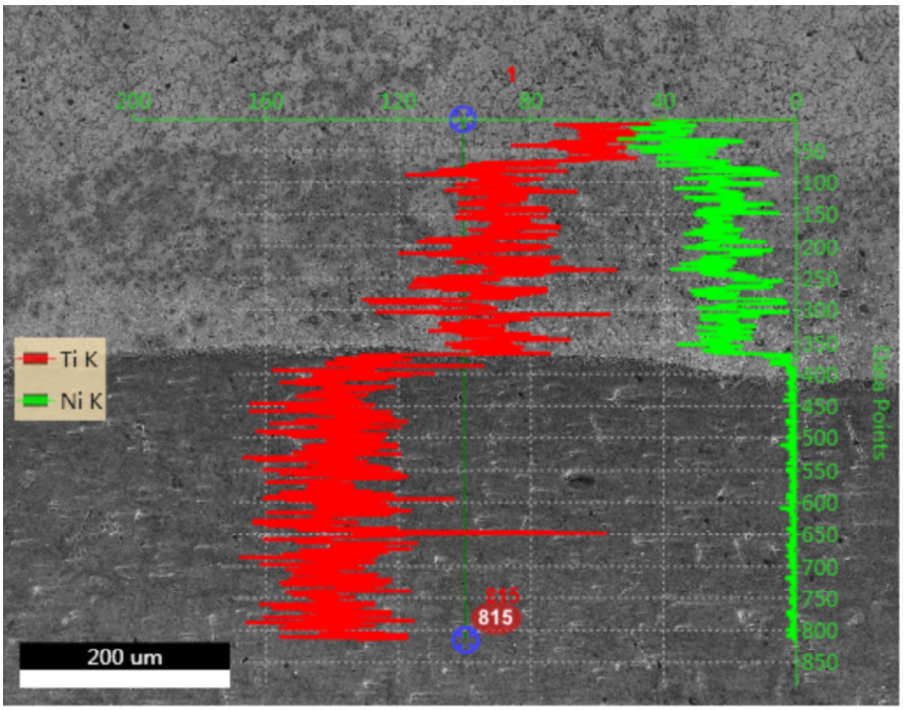

(**a**)

Figure 7. *Cont.*

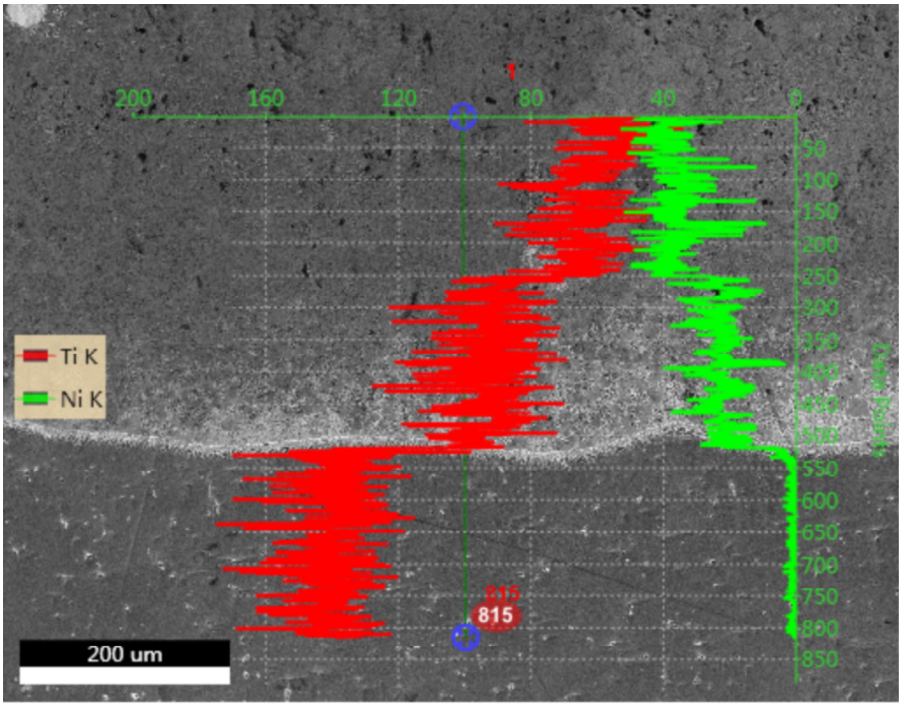

(**b**)

Figure 7. Line scan of elements near the fusion line. (**a**) Ni60 + 50% WC. (**b**) d22 priming + (Ni60 + 50% WC).

As can be seen from the graph, the diffusion of Ti and Ni in the Ni60 + 50% WC composite coating and the d22 primed + (Ni60 + 50% WC) composite coating is similar; taking coating A as an example, both elements show a step change at the interface, with the Ti content increasing from the starting point to the substrate, while the Ni content gradually decreases from the starting point to almost zero in the substrate. The diffusion between the clad material and the substrate promotes the formation of metallurgical bonds. The Ti content shows a step change in the transition layer area, especially at the interface, indicating that the alloying elements diffuse to different degrees at the interface, thus proving that the substrate and the coating have a reliable metallurgical bond at the interface.

3.3. Microhardness Analysis

In the direction of the coating cross-section, the microhardness varies in the direction of the substrate, as shown in Figure 8 (tested at 0.05 mm intervals along the coating toward the substrate and averaged over three points measured horizontally at the same depth, with the junction between the substrate and the coating as the zero point). It can be seen that the cross-section of the coating can be divided into three zones according to hardness: the substrate, the transition zone, and the cladding zone, with a gradient in hardness. The surface hardness values of the Ni60 + 50% WC composite coating are basically stable at around 947 ± 4 HV. The priming and surface hardness values of the d22 priming + (Ni60 + 50% WC) are stable at about 849 ± 4 HV and 929 ± 4 HV, respectively. In addition, the HAZ is subject to the diffusion of elements such as Ni and W, which increases its hardness to around 483 ± 3 HV. The d22 primed + (Ni60 + 50% WC) composite coating and Ni60 + 50% WC composite coating were compared with the TC4 titanium alloy substrate at the same time; Ni60 + 50% WC composite coating surface hardness values were higher than the TC4 titanium alloy substrate and had a large increase and more uniform distribution, being 2.82 times the TC4 titanium alloy substrate (336 ± 3 HV). The significant increase in microhardness of both coatings can be attributed to many WC particles and challenging phases such as W2C, TiC, and Ni17W3 in the coatings, and the intermetallic

compounds in the coatings' impeding dislocation movement, which further increases the microhardness of the coatings [19]. On the other hand, according to the alloy solidification theory, at the top of the cladding layer temperature gradient G → 0, solidification rate R → ∞ subcooling is larger. The grains do not have time to grow before they are generated; therefore, the grain size obtained is more uniform, fine, and dense. According to the delicate grain strengthening mechanism, the refined grains can improve the microhardness of the coating [20].

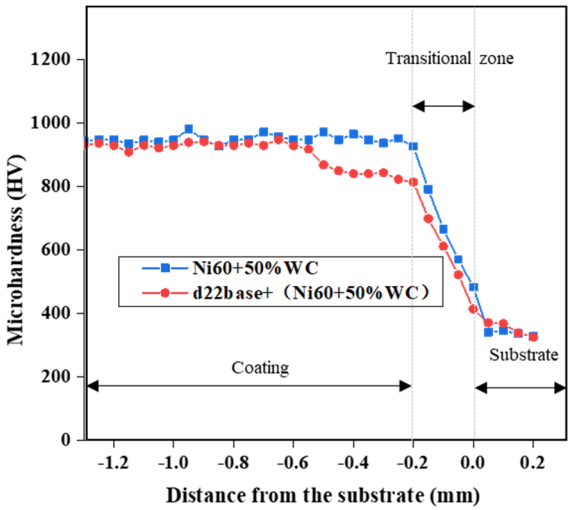

Figure 8. Plot of the microhardness of the coating on the cross section.

3.4. Dry Sliding Wear Study

Using the HRS-2M high-speed reciprocating friction and wear tester, the Ni60 + 50% WC composite coating, the d22 priming + (Ni60 + 50% WC) composite coating, and the TC4 titanium alloy substrate were subjected to wear test experiments at room temperature. The friction coefficient with the time curve is shown in Figure 9; from the figure, the turn of the friction coefficient with the change in time can be divided into two stages. Initially, the friction coefficient showed apparent fluctuations and was obviously in the wear run and location. After about 5 min, the friction coefficients of the two coatings fluctuated relatively little and were in the stable wear stage, while the substrate reached the stable wear stage only after about 10 min. The variation in the coefficient of friction for both coatings is somewhat more durable than the substrate, which may be due to the relatively hard coating. From Figure 10, it can be seen that the average coefficients of friction for the Ni60 + 50% WC composite coating, the d22 priming + (Ni60 + 50% WC) composite coating, and the TC4 titanium alloy substrate are 0.476, 0.55, and 0.865, respectively. Furthermore, it can also be observed from the graph that the coefficient of friction between the substrate and the coating gradually increases with growing friction time, probably because the surface temperature of the layer increases with rising wear time and because debris is not easily discharged from the friction area; this is due to the limitations of the friction device and more and more debris being pressed into the friction area, increasing the coefficient of friction [21]. The friction coefficient of Ni60 + 50% WC composite coating and d22 priming + (Ni60 + 50% WC) composite coating is much lower than that of the TC4 titanium alloy substrate, mainly due to the unfused WC particles in the layer and the in situ formation of enhanced phases W_2C, TiC, $Ni_{17}W_3$, Ni_3Ti, and Ti_xW_{1-x} acting as a "skeleton", which can effectively prevent microscopic cutting and thus improve the anti-wear performance of the coating.

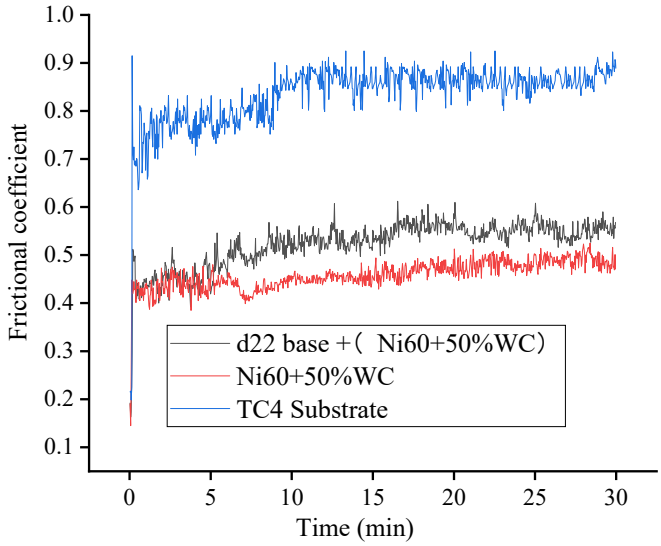

Figure 9. Friction coefficient—time curve.

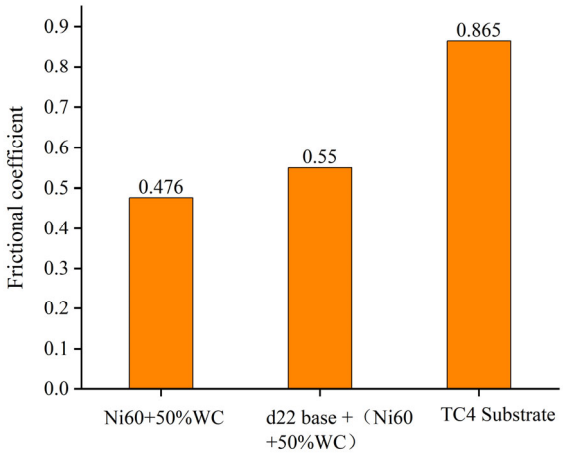

Figure 10. The average friction coefficient of the material.

The wear area is measured by the surface profiler, which in turn gives the wear volume (wear volume) as shown in Figure 11, from which it can be seen that the wear volumes of the Ni60 + 50% WC composite coating, the d22 priming + (Ni60 + 50% WC) composite layer, and the TC4 titanium alloy substrate are 0.1787 mm^3, 0.2458 mm^3, and 3.1955 mm^3 in that order. The wear of the TC4 titanium alloy substrate is 17.88 times greater than that of the Ni60 + 50% WC composite coating and 13 times greater than that of the d22 primed + (Ni60 + 50% WC) composite coating. This is mainly because the microstructure of the Ni60 + 50% WC composite coating is free from defects such as porosity and is more uniform and dense than the d22 primed + (Ni60 + 50% WC) composite layer, in addition to the relatively high hardness of the Ni60 + 50% WC composite coating.

Three-dimensional views, wear curves, and SEM morphologies of the wear surfaces of the Ni60 + 50% WC composite coating, the d22 priming + (Ni60 + 50% WC) composite layer, and the TC4 titanium alloy substrate after wear testing are shown in Figure 12. Combined with Figure 13 EDS Spot Results, the EDS energy spectrum results listed in Table 3 were combined to analyze further the wear mechanisms of the TC4 titanium alloy substrate and the Ni60 + 50% WC composite coating, B.

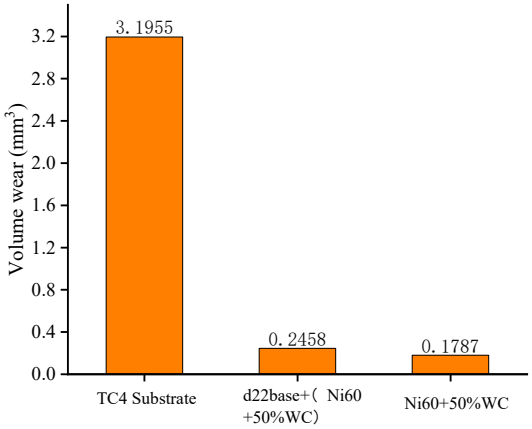

Figure 11. Wear of substrate and coating.

Table 3. Energy spectrum results for worn surfaces.

Sample Name	Phase	Mole Fraction/%								
		W	C	Ti	Al	Ni	V	O	Cr	N
Substrate	1	—	7.01	50.63	6.23	—	2.20	18.77	—	15.16
Coating A	2	81.46	11.15	2.23	—	2.78	—	4.62	—	—
	3	41.99	7.85	7.44	—	31.83	1.78	6.83	2.28	—
	4	54.32	15.12	2.75	—	3.77	—	24.04	—	—
	5	42.13	8.19	6.75	1.94	28.96	1.01	1.45	1.57	—
Coating B	6	9.47	12.19	10.83	1.78	33.99	—	31.74	—	—
	7	1.95	8.66	14.32	—	73.11	—	1.96	—	—
	8	42.23	8.12	15.25	—	26.61	1.25	5.19	1.35	—

From Figure 12(a1–a3), it is clear that some features appear on the surface of the worn TC4 titanium alloy substrate, such as many deep grooves parallel to the sliding direction as well as abrasive chips. The wear profile is deep and wide, with depths of up to 308 μm. This is mainly due to the low hardness of the TC4 titanium alloy substrate (approx. 336 ± 3 HV) and the ease with which the hard YG6 tungsten carbide beads penetrate the relatively soft surface of the substrate, where the slip lines and alternating stresses on the smooth surface of the substrate have continuous plastic shear, resulting in deep grooves and wear debris [21]. As shown in Figure 13, combined with the EDS results of Point 1, which has a high elemental O content, it is evident that the wear mechanism of the TC4 titanium alloy substrate is dominated by adhesive and abrasive wear, with oxidative wear also occurring. As can be seen from Figure 12(b1–b3), the Ni60 + 50% WC composite coating is characterized by scarring, a small amount of abrasion, and flaking on the surface after wear, but the grooves are non-existent, with only tiny shallow scratches and a wear depth of approximately 50 μm. The d22 priming + (Ni60 + 50% WC) composite coating can be observed after wearing with apparent features such as lamellar peeling, flaking, and shallow grooving (Figure 12(c1–c3)), with a wear depth of approximately 65 μm. Combined with its energy spectrum analysis, the high elemental oxygen content in the Point 4 and Point 6 sections, both coatings undergo oxidative wear; this is mainly attributed to the high temperature generated at the contact between the YG6 tungsten carbide steel beads and the surface of the wear layer in the case of high-speed reciprocal abrasive wear, causing the abrasive chips to oxidize and soften and adhere to the surface. It can be seen that the wear mechanisms of both the Ni60 + 50% WC composite coating and the d22 priming + (Ni60 + 50% WC) composite coating are dominated by adhesive and fatigue wear, with the occurrence of both abrasive and oxidative wear.

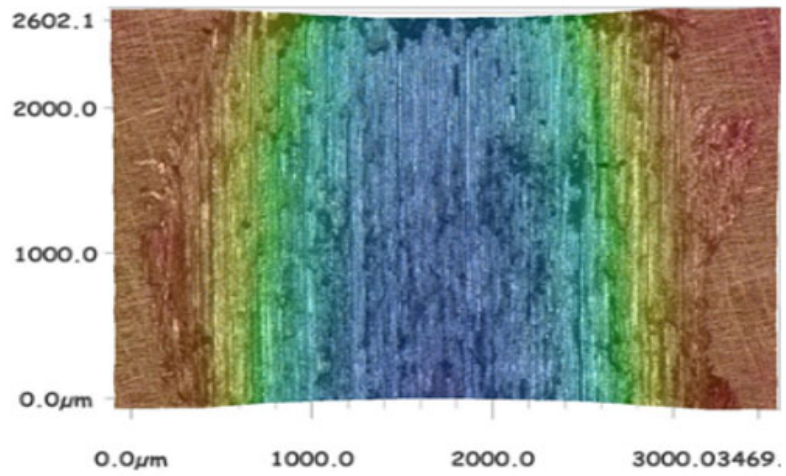

(**a1**)

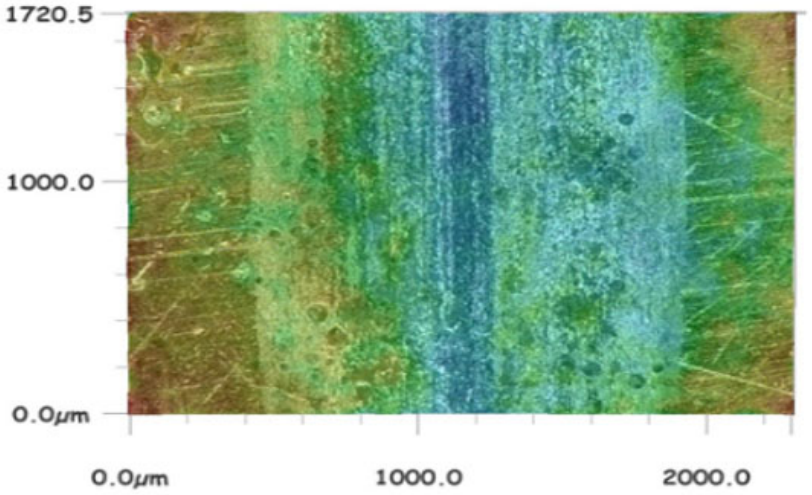

(**b1**)

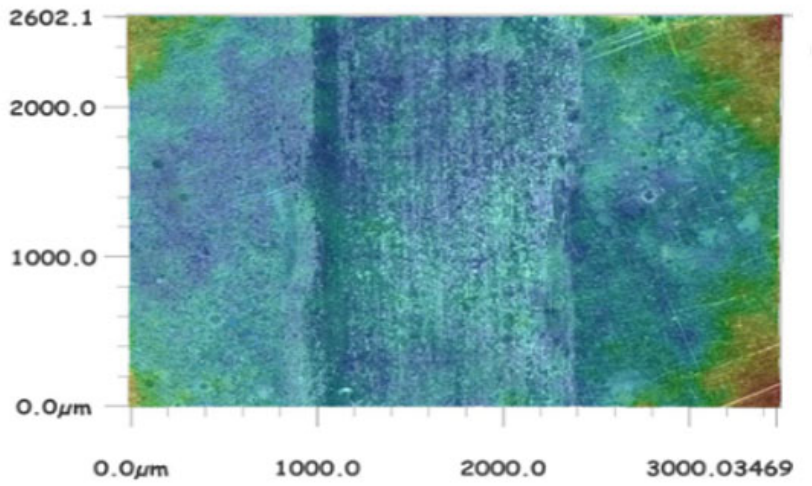

(**c1**)

Figure 12. *Cont.*

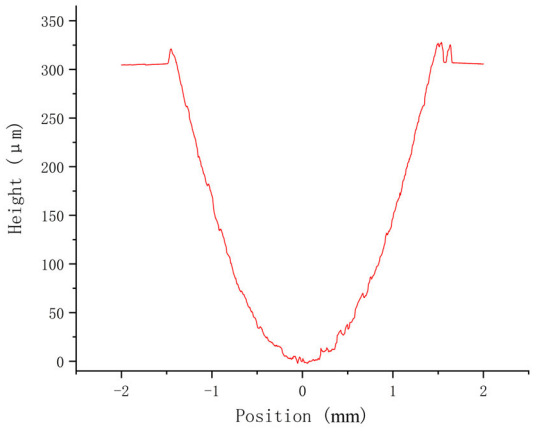

(**a2**)

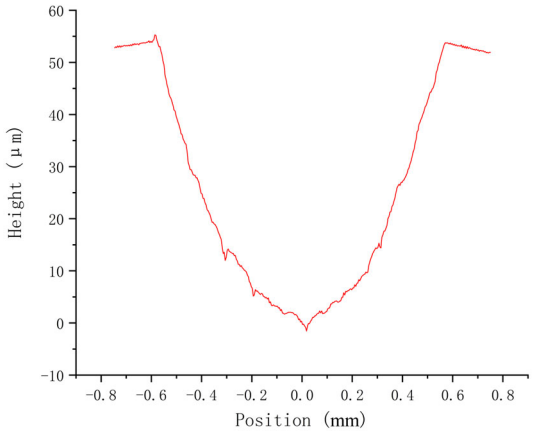

(**b2**)

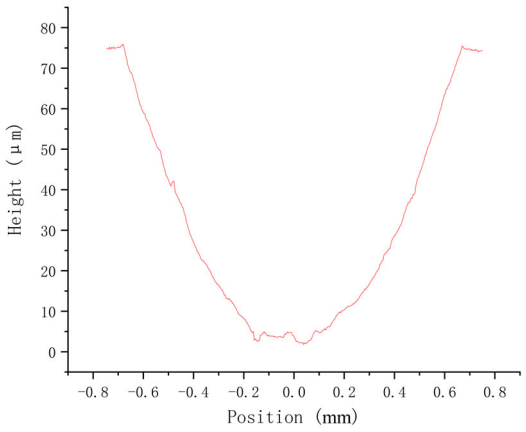

(**c2**)

Figure 12. *Cont.*

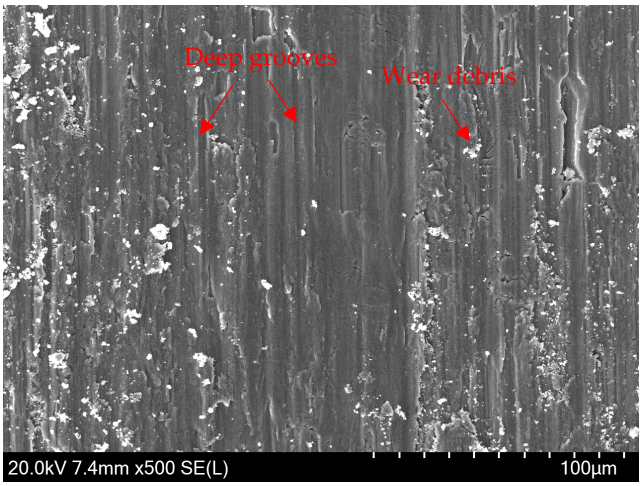

(**a3**)

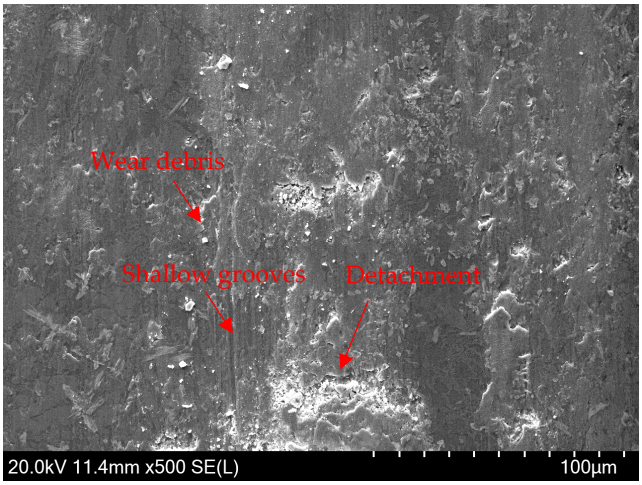

(**b3**)

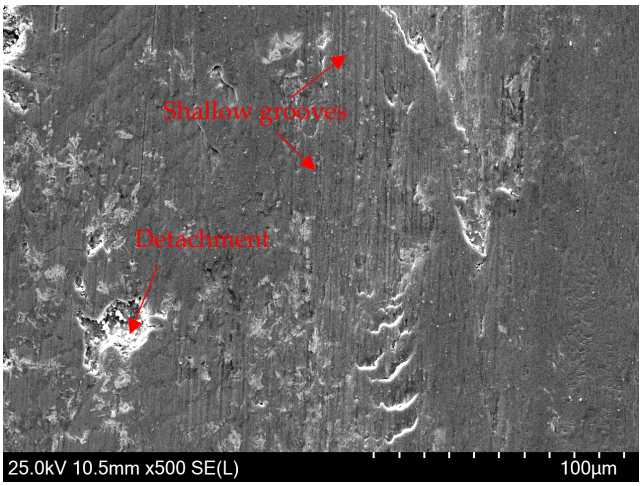

(**c3**)

Figure 12. Three-dimensional view, wear curve, and SEM profile of the worn surface. (**a1**–**a3**) TC4 titanium alloy substrate; (**b1**–**b3**) Ni60 + 50% WC composite coating; (**c1**–**c3**) d22 priming + (Ni60 + 50% WC) composite coating.

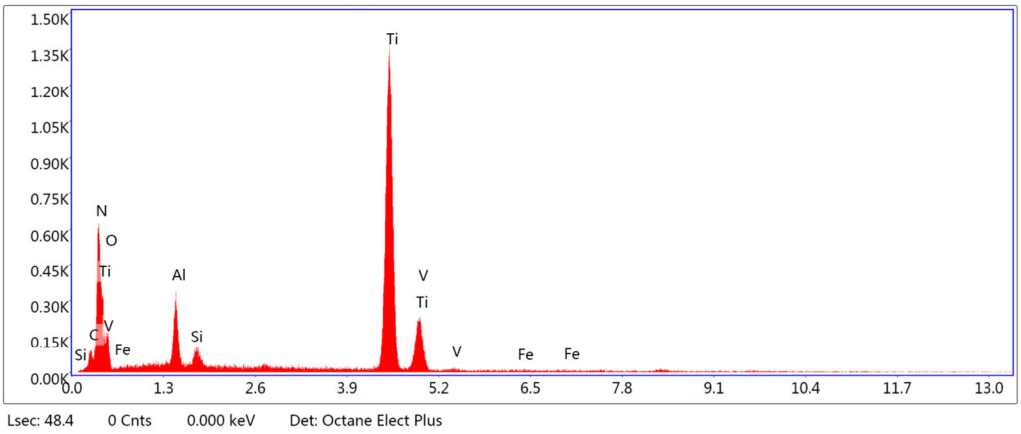

(**a**)

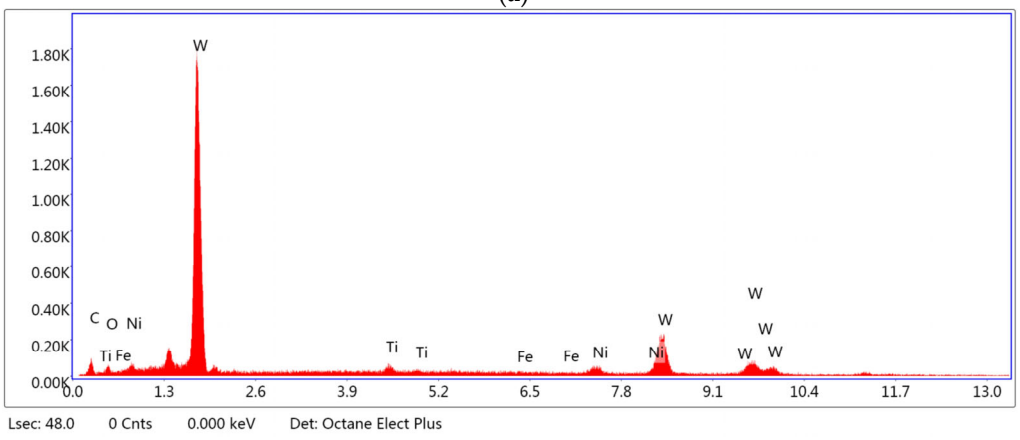

(**b**)

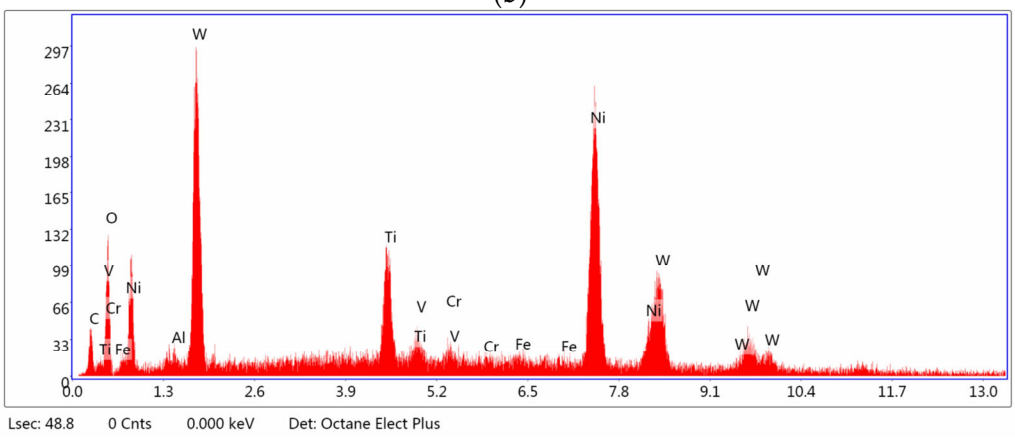

(**c**)

Figure 13. *Cont.*

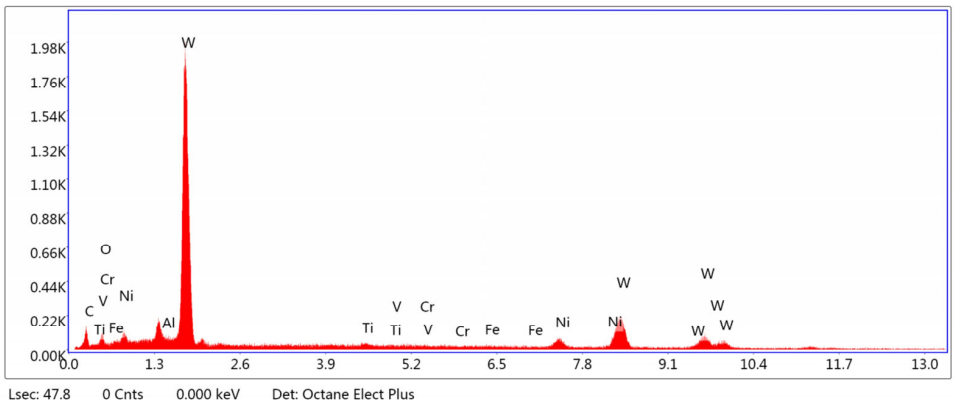

(**d**)

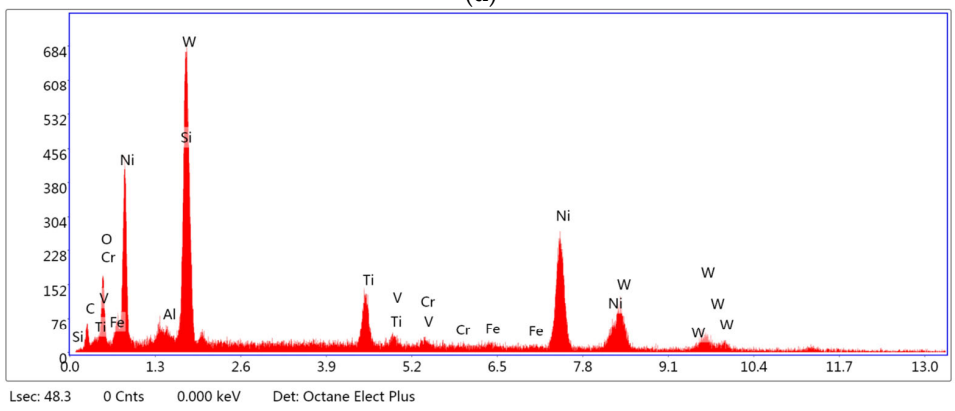

(**e**)

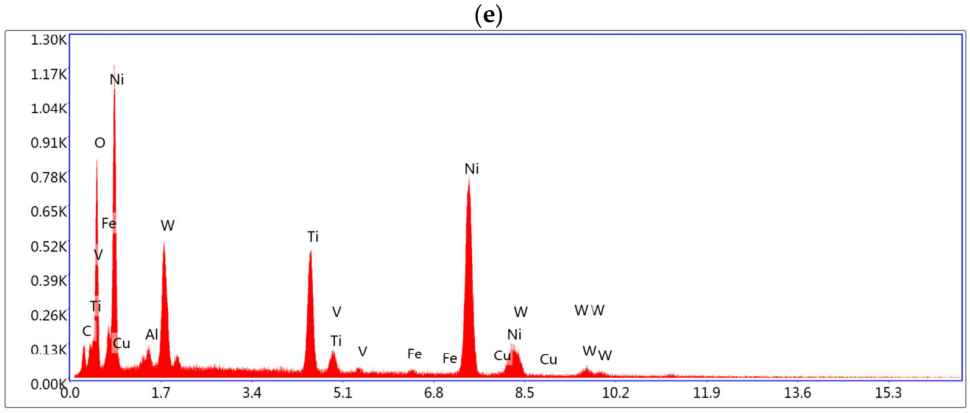

(**f**)

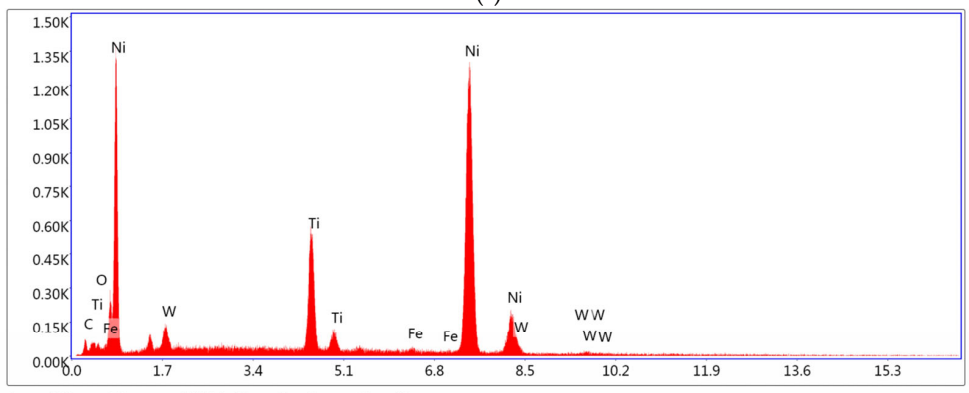

(**g**)

Figure 13. *Cont.*

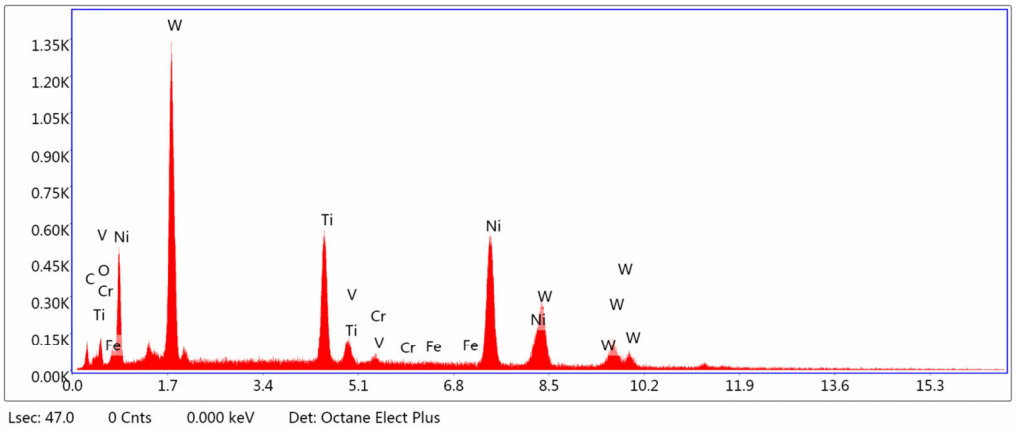

(**h**)

Figure 13. EDS Spot Results. (**a**) EDS Spot 1. (**b**) EDS Spot 2. (**c**) EDS Spot 3. (**d**) EDS Spot 4. (**e**) EDS Spot 5. (**f**) EDS Spot 6. (**g**) EDS Spot 7. (**h**) EDS Spot 8.

Compared to the substrate, the wear surface of both coatings is relatively flat and smooth, and the grooves are significantly shallower and narrower. This is mainly because during the wear test between the coating and the YG6 tungsten carbide steel beads, the unfused WC particles and the in situ formation of reinforcing phases such as W_2C, TiC, Ni_3Ti, and $Ni_{17}W_3$ act as a "skeleton" to prevent further wear and deformation of the coating effectively [22]; on the other hand, the high hardness of the layer also plays a positive role in enhancing the wear resistance [23].

3.5. Combined Strength Analysis

Record the change curve of pressure load and displacement during the shear process. When the coating is peeled off from the TC4 titanium alloy substrate under the action of shear force, measure the pressure load F. The calculation formula for coating bonding strength is as follows:

$$\sigma = \frac{F}{A} \tag{1}$$

where σ is the bonding strength of the coating; F is the pressure load when the layer is peeled off; and A is the area of the bonding zone.

Figure 14 shows the relationship between the pressure load applied by the instrument indenter and its displacement during the loading process. During the contact pressure stage of the pressure head, the deformation of Ni60 + 50% WC increases faster and the pressure rises slower, while the pressure of d22 substrate + (Ni60 + 50% WC) increases faster. Table 4 shows the specific data for the bond strength of the coating, calculated using Equation (1).

Table 4. Experimental data on shear bond strength.

Sample Name	Pressure Load F (N)	Bonding Area A (mm^2)	Shear Bond Strength σ (MPa)
Coating A	18,443	98	188.19
Coating B	4813	98	49.11

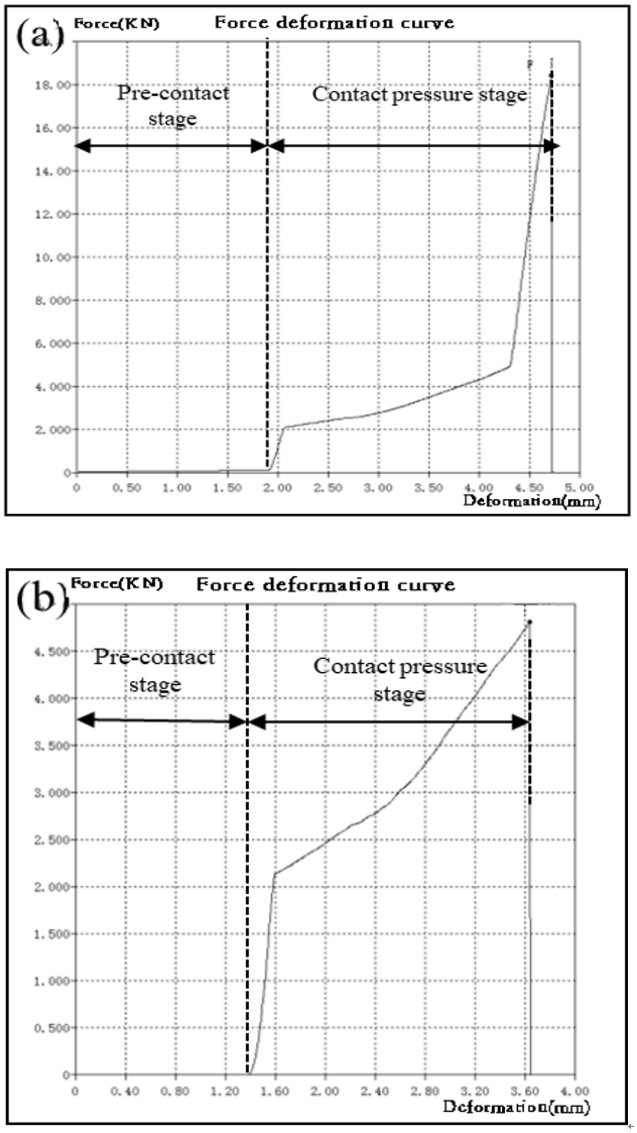

Figure 14. Pressure load–displacement curve: (**a**) Ni60 + 50% WC, (**b**) d22 priming + (Ni60 + 50% WC).

As can be seen from the table, the shear bond strengths of Ni60 + 50% WC and d22 priming + (Ni60 + 50% WC) are 188.19 MPa and 49.11 MPa, respectively. The bond strength of the d22 primed + (Ni60 + 50% WC) composite coating is much lower than that of the Ni60 + 50% WC composite coating because (1) there are obvious defects, such as holes and pinholes in the d22 primed + (Ni60 + 50% WC) composite coating; and (2) the d22 primed layer (about 0.6 mm) is too thick and easily makes the interface brittle, which in turn leads to low bond strength [24]. A strong shear bond between the coating and the substrate enhances the overall integrity of the coating system. It helps to distribute loads evenly across the surface, reducing the risk of localized damage or failure. This is especially important in coatings used for structural or protective purposes, where the coating acts as a barrier against external factors such as corrosion, abrasion, or impact. The Ni60 + 50% WC composite coating will exhibit better results.

4. Conclusions

(1) The Ni60 + 50% WC composite coating and the d22 primed + (Ni60 + 50% WC) composite coating have a physical phase consisting of W_2C, TiC, $Ni_{17}W_3$, Ni_3Ti, and Ti_xW_{1-x}. Both coatings show excellent metallurgical bonding with the TC4 titanium

alloy substrate, and no cracking defects were observed, but the d22 primed + (Ni60 + 50% WC) composite coating has significant porosity defects.

(2) The surface microhardness of the Ni60 + 50% WC composite coating and the d22 substrate + (Ni60 + 50% WC) composite coating is approximately 947.06 HV and 848.65 HV-928.89 HV, respectively, which is about 2.52–2.82 times that of the substrate (336.43 HV). The significant increase in the microhardness of both coatings is primarily due to the presence of hard phases such as W_2C, TiC, Ni_3Ti, and the combined effect of grain refinement.

(3) The average coefficients of friction for the Ni60 + 50% WC composite coating, the d22 substrate + (Ni60 + 50% WC) composite coating, and the TC4 titanium alloy substrate are 0.476, 0.55, and 0.865, respectively. The wear volumes are 0.1787 mm^3, 0.2458 mm^3, and 3.1955 mm^3, respectively. The wear volume of the TC4 titanium alloy substrate is 17.88 times that of the Ni60 + 50% WC composite coating and 13 times that of the d22 substrate + (Ni60 + 50% WC) composite coating, indicating a significant improvement in wear resistance. According to the results of the wear surfaces, the wear mechanisms of both the Ni60 + 50% WC composite coating and the d22 substrate + (Ni60 + 50% WC) composite coating are mainly adhesive wear and fatigue wear, with the occurrence of abrasive wear and oxidative wear as well.

(4) The interface shear test shows that the shear bonding strength of Ni60 + 50% WC and d22 substrate + (Ni60 + 50% WC) is 188.19 MPa and 49.11 MPa, respectively. The d22 primer + (Ni60 + 50% WC) composite coating has low bonding strength due to the presence of pores, pinhole defects, and a thick primer layer.

(5) By comparing the performance of Ni60 + 50% WC composite coating and d22 base + (Ni60 + 50% WC) composite coating through experimental results, Ni60 + 50% WC composite coating performs better than d22 base + (Ni60 + 50% WC) composite coating and substrate in terms of hardness, wear resistance, and shear bonding strength.

Author Contributions: Conceptualization, G.W.; Methodology, J.L.; Validation, J.Y.; Formal analysis, S.L.; Resources, J.C.; Data curation, L.B. All authors have read and agreed to the published version of the manuscript.

Funding: This research was funded by the National Natural Science Foundation of China (52075465), Hunan Provincial Science and Technology Innovation Program (2020RC4038), Hunan Provincial Natural Science Foundation of China (2021J50110), and Key Products of Hunan Province's Manufacturing Industry "Unveiled and Leading" Project (2023GXGG018).

Institutional Review Board Statement: Not applicable.

Informed Consent Statement: Not applicable.

Data Availability Statement: Data are contained within the article.

Conflicts of Interest: Author Jianwen Chen was employed by the company Jianglu Machinery Group Co. Ltd. The remaining authors declare that the research was conducted in the absence of any commercial or financial relationships that could be construed as a potential conflict of interest.

References

1. Wang, Y.; Li, J.; Dang, C.; Wang, Y.; Zhu, Y. Influence of carbon contents on the structure and tribocorrosion properties of TiSiCN coatings on Ti6Al4V. *Tribol. Int.* **2017**, *109*, 285–296. [CrossRef]
2. Jin, H.X.; Wei, K.X.; Li, J.M.; Zhou, J.Y.; Peng, W.J. Research development of titanium alloy in aerospace industry. *Chin. J. Nonferrous Met.* **2015**, *25*, 280–292.
3. Xu, J.; Liu, X.; Qiao, S.; Zhai, Y.; Tu, R. Microstructure and high-temperature oxidation resistance of NiCrAlSi composite coating on Ti6Al4V alloy by laser cladding. *Chin. J. Nonferrous Met.* **2018**, *28*, 46–52.
4. Yuan, Y.G.; Kang, J.J.; Yue, W.; Fu, Z.Q.; Zhu, L.N.; She, D.S. Tribological properties of TC4 titanium alloy treated by plasma nitriding at different temperatures. *J. Mater. Eng.* **2020**, *48*, 156–162.
5. Farotade, G.A.; Adesina, O.S.; Foluso Ogunbiyi, O.; Tobi Adesina, O.; Kazeem, R.A.; Adeniran, A.A. Microstructural characterization and surface properties of laser clad Ni-ZrB2 coatings on Ti-6Al-4V alloy. *Mater. Today Proc.* **2021**, *38*, 1035–1039. [CrossRef]

6. Bansal, P.; Singh, G.; Sidhu, H.S. Improvement of surface properties and corrosion resistance of Ti13Nb13Zr titanium alloy by plasma-sprayed HA/ZnO coatings for biomedical applications. *Mater. Chem. Phys.* **2021**, *257*, 123738. [CrossRef]
7. Yang, C.; Cheng, X.; Tang, H.; Tian, X.; Liu, D. Influence of microstructures and wear behaviors of the microalloyed coatings on TC11 alloy surface using laser cladding technique. *Surf. Coat. Technol.* **2018**, *337*, 97–103. [CrossRef]
8. Shen, J.; Zou, B.; Cai, X.; Dong, S.; Cao, X. Fabrication and properties of TiB2-TiC reinforced NiAl coatings by reactive plasma spraying on AZ91D magnesium alloy. *Surf. Coat. Technol.* **2019**, *378*, 125055. [CrossRef]
9. Peng, Y.; Zhang, W.; Li, T.; Zhang, M.; Wang, L.; Song, Y.; Hu, S.; Hu, Y. Microstructures and mechanical properties of FeCoCrNi high entropy alloy/WC reinforcing particles composite coatings prepared by laser cladding and plasma cladding. *Int. J. Refract. Met. Hard Mater.* **2019**, *84*, 105044. [CrossRef]
10. Gao, Z.; Tan, J.; Guo, W.; Zhang, C. Effect of Ni-based and Fe-based Laser Cladding Materials on Microstructure and Property of Cladding Layer. *Hot Work. Technol.* **2017**, *46*, 161–164. [CrossRef]
11. Li, L.; Liu, D.; Chen, Y.; Wang, C.; Li, F. Electron microscopy study of reaction layers between single-crystal WC particle and Ti–6Al–4V after laser melt injection. *Acta Mater.* **2009**, *57*, 3606–3614. [CrossRef]
12. Wang, X.; Zhou, S.; Dai, X.; Lei, J.; Guo, J.; Gu, Z.; Wang, T. Evaluation and mechanisms on heat damage of WC particles in Ni60/WC composite coatings by laser induction hybrid cladding. *Int. J. Refract. Met. Hard Mater.* **2017**, *64*, 234–241. [CrossRef]
13. Chen, Y.; Newkirk, J.W.; Liou, F. Synthesizing Ti–Ni Alloy Composite Coating on Ti–6Al–4V Surface from Laser Surface Modification. *Metals* **2023**, *13*, 243. [CrossRef]
14. Chen, Y. Study on Wear Resistance of Ni-based Alloy Coating Reinforced with WC Particles by Laser Cladding. *Hot Work. Technol.* **2022**, *51*, 106–109. [CrossRef]
15. Guo, C.; Chen, J.; Zhou, J.; Zhao, J.; Wang, L.; Yu, Y.; Zhou, H. Effects of WC–Ni content on microstructure and wear resistance of laser cladding Ni-based alloys coating. *Surf. Coat. Technol.* **2012**, *206*, 2064–2071. [CrossRef]
16. Wang, K.; Liu, W.; Li, X.; Tong, Y.; Hu, Y.; Hu, H.; Chang, B.; Ju, J. Effect of hot isostatic pressing on microstructure and properties of high chromium K648 superalloy manufacturing by extreme high-speed laser metal deposition. *J. Mater. Res. Technol.* **2024**, *28*, 3951–3959. [CrossRef]
17. Van Acker, K.; Vanhoyweghen, D.; Persoons, R.; Vangrunderbeek, J. Influence of tungsten carbide particle size and distribution on the wear resistance of laser clad WC/Ni coatings. *Wear* **2005**, *258*, 194–202. [CrossRef]
18. Li, J.; Chen, C.; Lin, Z.; Squartini, T. Phase constituents and microstructure of laser cladding Al_2O_3/Ti_3Al reinforced ceramic layer on titanium alloy. *J. Alloys Compd.* **2011**, *509*, 4882–4886. [CrossRef]
19. Tao, X.; Zhang, S.; Zhang, C.; Wu, C.; Chen, J.; Abdullah, A.O. Effect of Fe and Ni contents on microstructure and wear resistance of aluminum bronze coatings on 316 stainless steel by laser cladding. *Surf. Coat. Technol.* **2018**, *342*, 76–84. [CrossRef]
20. Duan, X.; Gao, S.; Dong, Q.; Zhou, Y.; Xi, M.; Xian, X.; Wang, B. Reinforcement mechanism and wear resistance of Al2O3/Fe-Cr-Mo steel composite coating produced by laser cladding. *Surf. Coat. Technol.* **2016**, *291*, 230–238. [CrossRef]
21. Gao, Q.; Yan, H.; Qin, Y.; Zhang, P.; Guo, J.; Chen, Z.; Yu, Z. Laser cladding Ti-Ni/TiN/TiW+TiS/WS2 self-lubricating wear resistant composite coating on Ti-6Al-4V alloy. *Opt. Laser Technol.* **2019**, *113*, 182–191. [CrossRef]
22. Wang, K.; Liu, W.; Hong, Y.; Shakhawat, S.; Tong, Y.; Hu, Y.; Zhang, M.; Zhang, J.; Xiang, D.; Fu, H.; et al. An Overview of Technological Parameter Optimization in the Case of Laser Cladding. *Coatings* **2023**, *13*, 496. [CrossRef]
23. Xue, J.; Guo, W.; Yang, J.; Xia, M.; Zhao, G.; Tan, C.; Wan, Z.; Chi, J.; Zhang, H. In-situ observation of microcrack initiation and damage nucleation modes on the HAZ of laser-welded DP1180 joint. *J. Mater. Sci. Technol.* **2023**, *148*, 138–149. [CrossRef]
24. Su, X.; Zhang, X. Interfacial Bonding Strength between Surface Coating and Substrate and Its M easurement. *Electroplat. Pollut. Control.* **2004**, *24*, 6–11.